JNP Journal of Nanophotonics

RESEARCH PAPER

Anisotropic absorption enhancement in hybrid black phosphorous-plasmonic nanograting systems

Shinpei Ogawa,* Manabu Iwakawa, Shoichiro Fukushima, and Masaaki Shimatani

Mitsubishi Electric Corporation, Advanced Technology R&D Center, Amagasaki, Japan

ABSTRACT. Although black phosphorous (BP) is a promising two-dimensional material for next-generation infrared (IR) photodetectors, enhancing its quantum efficiency remains challenging. We propose a hybrid BP/plasmonic nanograting with a narrow width and a high-depth groove system to address this challenge. The absorption properties of BP formed on plasmonic nanograting systems with two configurations, namely, an armchair edge normal and parallel to the groove direction, were numerically investigated. These systems demonstrated polarization-selective, wide-angle, near-unity absorption in the IR-wavelength region, and the absorption wavelength was controlled primarily by the groove depth. The BP induced a blue shift of the absorption wavelength, and the wavelength shift was larger for the armchair edge that was normal to the groove direction than that parallel to the groove direction. These results can be attributed to the coupling between the anisotropic surface plasmon resonances of BP and the plasmonic nanogratings. Moreover, this wavelength shift was enhanced by an increase in the carrier density of BP. The BP carrier density can be controlled by its electrical gating. This implies that the detection wavelength can be controlled by electrical gating of the BP. These systems can contribute to the development of high-performance BP-based polarization-selective and/or wavelength-tunable advanced IR photodetectors.

Keywords: black phosphorous; 2D materials; plasmonics; metasurfaces; metamaterials

Paper 24101G received Oct. 11, 2024; revised Dec. 19, 2024; accepted Jan. 6, 2025; published Jan. 27, 2025.

1 Introduction

Atomically thin two-dimensional (2D) materials such as graphene,[1,2] hexagonal boron nitride,[3,4] transition-metal dichalcogenides,[5] and black phosphorous (BP)[6,7] have attracted significant attention for use in optical devices such as photodetectors, which operate in various wavelength regions. Graphene demonstrates significant potential for use in high-performance photodetectors.[8–11] However, graphene is a semi-metal with no bandgap, thus resulting in a large dark current and poor photodetector performance. BP is a 2D semiconductor with a layer-number-dependent direct bandgap that approximately corresponds to the middle-to-long wavelength infrared (IR) region, high carrier mobility, and high carrier density.[7] Moreover, BP exhibits a polarization dependence based on its in-plane anisotropy, which can result in unique polarization-dependent optical properties. Therefore, numerous studies have been conducted to develop high-performance BP-based IR

*Address all correspondence to Shinpei Ogawa, Ogawa.Shimpei@eb.MitsubishiElectric.co.jp

photodetectors by exploiting the unique properties of BP.[12–15] However, the inadequate quantum efficiency of BP is a critical limitation to overcome.

To address this challenge, the integration of BP with plasmonic nanostructures[16–18] or the formation of plasmonic structures on BP, e.g., BP-based nanoribbon,[19–21] are potential strategies. However, in the latter case, forming BP into a nanoribbon structure may induce defects that reduce the crystal quality of BP and, subsequently, lower the BP-based photodetector performance. Therefore, the former strategy was adopted in this study. Plasmonic nanostructures such as one-dimensional (1D) plasmonic gratings,[22,23] 2D plasmonic crystals,[24] metal-dielectric-metal,[25,26] bow-tie antennas,[13] and 3D metallic structures[27] can produce surface plasmon resonances (SPRs) and couple them with BP, which enhances the absorption of BP at the SPR wavelength. Furthermore, the asymmetric structure of plasmonic nanostructures induces polarization selectivity.[28] The hybrid plasmonic metasurface and BP can lead to unique phenomena related to light–matter interactions.[29]

In this study, a hybrid BP/plasmonic nanograting system was proposed to realize high-performance BP-based IR photodetectors. One-dimensional plasmonic nanogratings with high-aspect ratios, where the ratio of the depth and width of grooves is approximately larger than 10, exhibit incident-angle independence and strong near-unity absorption in the IR-wavelength region owing to localized SPR (LSPR). This absorption is determined only by the grating depth.[30–34] Conventional gratings exhibit strong incident angle dependence characteristics, and their absorption wavelengths depend on various parameters such as the grating period, width, and depth. Therefore, the plasmonic nanogratings have several advantages, such as the incident angle independence, and absorption wavelength tunability only as a function of the grating depth with strong absorbance (almost equal to unity). These properties are advantageous for various applications, such as IR photodetectors and IR absorbers/emitters. Therefore, hybrid BP/plasmonic nanogratings are expected to provide fundamental insights into the development of high-performance BP-based IR photodetectors, in addition to unique physics, given that both BP and plasmonic nanogratings exhibit anisotropy in terms of their structures and optical properties. The polarization-dependent absorbance of BP on plasmonic nanogratings was theoretically investigated using the rigorous coupled-wave analysis (RCWA)[35] method based on the anisotropic permittivity of BP. The optical interaction between the BP and plasmonic nanogratings was investigated according to the configuration of the anisotropic edge structure of the BP in the groove direction of the plasmonic nanogratings, which is defined as the direction normal to the pitch direction on the plasmonic nanograting surface. Furthermore, absorption modulation by the carrier density of BP was investigated. The obtained results demonstrate that anisotropic absorption occurs, as determined by the configuration of the edge structure of BP and the groove direction, and the modulation can be controlled by the carrier density of BP. This is direct evidence of the anisotropic coupling of SPRs between the BP and the plasmonic nanogratings.

2 Materials and Methods

2.1 Materials

Figure 1 presents a schematic of monolayer BP. As shown in Fig. 1, BP has an asymmetric edge structure with an armchair edge and a zigzag edge in the X- and Y-directions, respectively.

Therefore, the permittivity of BP is anisotropic, as expressed by Eq. (1):

$$\epsilon_j = \epsilon_r + \frac{i\sigma_j}{\epsilon_0 \omega d}, \tag{1}$$

where ϵ_0 is the permittivity of free space, ω is the angular frequency, d is the thickness of BP, j denotes either the x-, y-, or z-directions, $\epsilon_r = 5.76$,[36] and σ_j is the asymmetric surface conductivity of BP. The in-plane (stacking direction) surface conductivity σ_z is close to zero.

The surface conductivity of BP, as calculated using the semiclassical Drude model, is expressed as follows:[37–39]

$$\sigma_j = \frac{iD_j}{\pi\left(\omega + \frac{i\eta}{\hbar}\right)}, \quad D_j = \frac{\pi e^2 n}{m_j}, \tag{2}$$

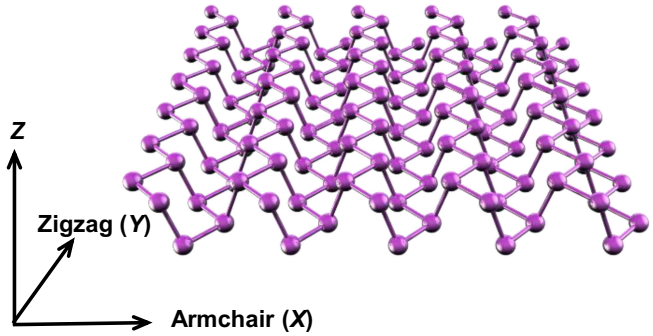

Fig. 1 Schematics of monolayer black phosphorus (BP) with armchair edge and zigzag edge.

where D_j is the Drude weight, η is the relaxation rate, n is the electron doping density, and e is the elementary charge. The parameter m_j denotes the electron mass in the X- or Y-directions and is given by Eq. (3)[38,39]

$$m_x = \frac{\hbar^2}{\frac{2\gamma^2}{\Delta} + \eta_c}, \quad m_y = \frac{\hbar^2}{2v_c}. \tag{3}$$

In the case of monolayer BP,[38,39]

$$\gamma = \frac{4a}{\pi}\ \text{eVm}, \quad \eta_c = \frac{\hbar^2}{0.4m_0}, \quad \nu_c = \frac{\hbar^2}{1.4m_0}. \tag{4}$$

The following values were used in these equations to obtain the anisotropic permittivity of BP: lattice constant $a = 0.223$ nm, bandgap $\Delta = 2$ eV, $m_0 = 9.10938 \times 10^{-31}$ kg, electron doping $n = 3.0 \times 10^{13}$ cm^{-2},[39] and $\eta = 10$ meV. For the monolayer BP, $d = 1$ nm.

2.2 Device Structures

We considered two types of device structures to investigate the effect of the anisotropic edges of BP. Figures 2(a) and 2(b) present schematics of the monolayer BP on the plasmonic

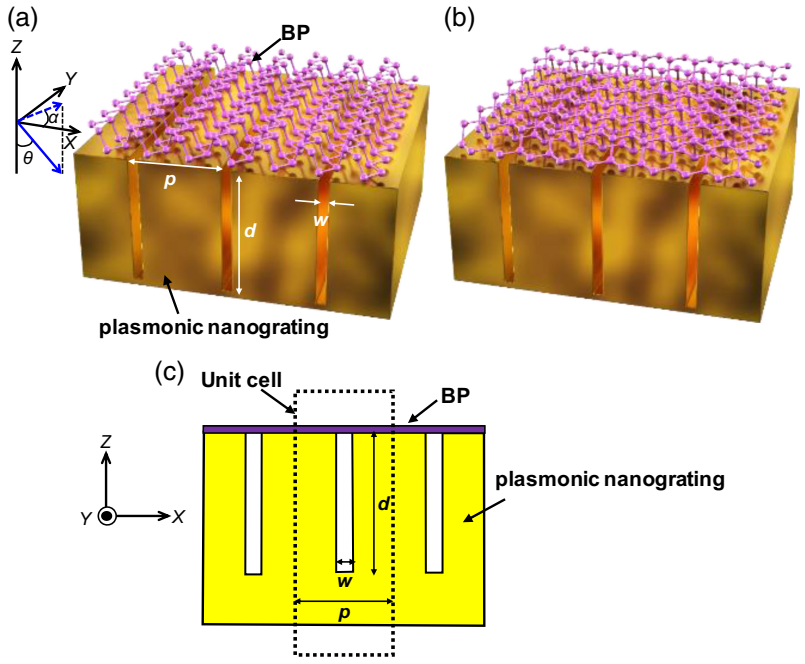

Fig. 2 Schematics of monolayer BP on a plasmonic nanograting with armchair and zigzag edges (a) in X- and Y-directions (BP-PN-A) and (b) in Y- and X-directions (BP-PN-B). (c) Schematic of the unit cell in the XZ plane used for calculations.

nanogratings, where the armchair and zigzag edge structures are oriented in the X- and Y-directions and the Y- and X-directions, respectively. In this study, the groove direction was defined as the Y-direction. Herein, the former and latter structures are referred to as "BP-PN-A" and "BP-PN-B," respectively. The plasmonic nanogratings were based on Au.

The width, depth, and period of the grooves were defined as w, d, and p, respectively, and w and p were fixed at 100 nm and 3.0 μm, respectively. The design parameter of the plasmonic nanogratings used in this study was determined by considering the fabrication procedure because the construction of plasmonic nanogratings with high-aspect ratios ($\geq$10) is difficult when conventional metal grating fabrication methods are used. We have demonstrated in a previous study the implementation of a plasmonic nanograting with $w = 100$ nm, $d = 1.5$ μm, and $p = 3.0$ μm using the tapered mold method.[33] Therefore, these values were mainly used in this numerical study. BP can be transferred on the plasmonic nanograting by using the dry transfer method (also used for graphene).[40] The incident light is indicated by a solid blue arrow in Fig. 2(a). The incident angle and polarization angle were defined using the symbols θ and α, respectively.

3 Results and Discussion

The absorption properties were calculated using the RCWA method. The permittivity of BP was obtained using Eqs. (1)–(4). The permittivity of Au was obtained from a previous study.[41] The polarization of the transverse magnetic (TM) mode with an α value of 0 deg was only considered in this study because the absorption of 1D plasmonic nanogratings is nearly zero for the polarization of the transverse electric (TE) mode with an α value of 90 deg.[33] The unit cell used in the calculation is shown in Fig. 2(c). As indicated, the unit cell is based on a three-dimensional (and not a two-dimensional) structure owing to the asymmetric structure of the BP in the XY plane. Hence, the variable p was used to define the unit sizes in both the X- and Y-directions. The unit size in the Z-direction was set at d with a distance of 2.5 μm above the top part of the groove, and a distance of 1.0 μm from the bottom part of the groove to the bottom part of the grating, which was adequately thick to block transmission. It was confirmed that the calculated absorption spectra do not change when the number of spatial harmonics is greater than nine, and the

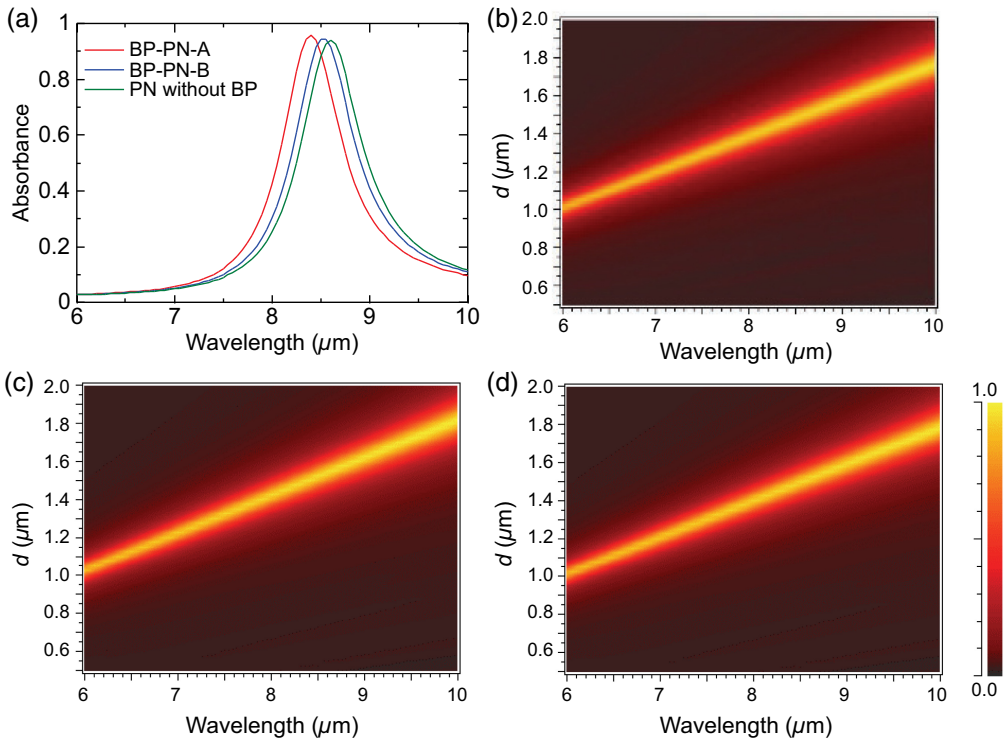

Fig. 3 (a) Calculated absorbance spectra with $d = 1.5$ μm for PN without BP, BP-PN-A, and BP-PN-B. Calculated absorbances as a function of wavelength and d for (b) PN without BP, (c) BP-PN-A, and (d) BP-PN-B. The color scale represents the absorbance.

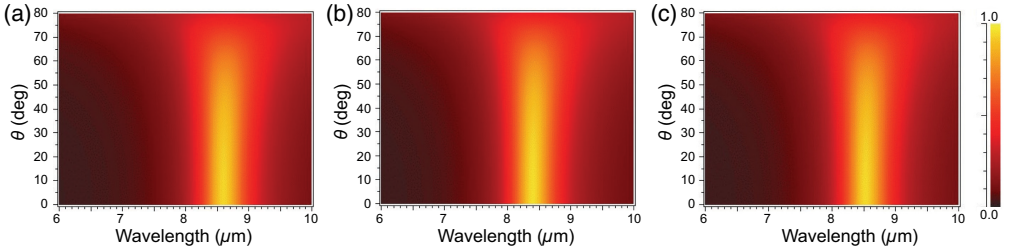

Fig. 4 (a) Calculated absorbances as a function of wavelength and θ for (a) PN without BP, (b) BP-PN-A, and (c) BP-PN-B. The color scale represents the absorbance.

calculated results are consistent with the experimental results.[33] Therefore, 10 spatial harmonics were used for RCWA calculations.

3.1 Effects of Anisotropic Edge Structure of BP on Absorption

Figure 3(a) presents the calculated absorbance spectra for BP-PN-A, BP-PN-B, and the plasmonic nanograting without BP (PN without BP), with $d = 1.5$ μm. Figures 3(b)–3(d) present the calculated absorbances as functions of the wavelength and d for PN without BP [Fig. 3(b)], BP-PN-A [Fig. 3(c)], and BP-PN-B [Fig. 3(d)]. Figures 3(b)–3(d) present the contour maps, where the absorbance increases from 0 to 1.0, corresponding to the color change from black to yellow.

Figure 3 reveals that a strong unity absorbance of over ~90% was obtained for all the structures, and the absorption wavelength was nearly proportional to d.[33] These characteristics can be mainly attributed to the LSPRs of the plasmonic nanogratings in the groove depth direction of the Z-axis. Figure 3(a) indicates that the maximum absorption wavelength exhibits an anisotropic shift from a wavelength of 8.60 μm to either 8.40 μm or 8.55 μm in the BP-PN-A and BP-PN-B cases, respectively. This is because LSPRs were induced by the plasmonic nanograting coupled with the anisotropic SPRs of BP to produce anisotropic wavelength shifts. Figures 4(a)–4(c) present the calculated absorbances as a function of wavelength and θ for PN without BP [Fig. 4(a)], BP-PN-A [Fig. 4(b)], and BP-PN-B [Fig. 4(c)], respectively.

Figure 4(a) reveals that the plasmonic nanograting has a unique absorption property of incident-angle independence. Figures 4(b) and 4(c) reveal that such incident-angle independence was maintained, even with BP forming on the plasmonic nanogratings. However, the maximum absorption wavelength was shifted according to the anisotropic edge structures of the BP. These results reveal that hybrid BP/plasmonic nanograting systems produce incident-angle-insensitive and near-unity absorption in the IR wavelength region (which can only be determined by d) and modify the absorption wavelength by the configuration of the anisotropic edge of the BP and the groove direction. This can be attributed to the strong coupling of the SPRs of both the plasmonic nanogratings and BP.

3.2 Tunable Absorption Wavelength by Carrier Density of BP

The effect of carrier density n was investigated. In this section, an increased value of $n = 1.0 \times 10^{14}$ cm^{-2} was used. Figure 5(a) presents the calculated absorbance spectra of BP-PN-A, BP-PN-B, and PN without BP with $d = 1.5$ μm. Figures 5(b) and 5(c) present the calculated absorbances as functions of the wavelength and d for BP-PN-A and BP-PN-B, respectively.

Figures 6(a) and 6(b) present the calculated absorbances as a function of wavelength and θ for BP-PN-A and BP-PN-B, respectively.

Figures 5 and 6 reveal that the absorption wavelength is proportional to d, and the absorption wavelength is independent of the incident angle. As shown in Fig. 5(a), the maximum absorption wavelength shifted from 8.60 μm to 8.00 μm and 8.30 μm in the BP-PN-A and BP-PN-B cases, respectively. The absorption wavelengths decreased following an increase in n from 3.0×10^{13} cm^{-2} to 1.0×10^{14} cm^{-2}. These results provide direct evidence of the coupling of LSPRs by the plasmonic nanogratings and SPRs of BP, given that the SPR wavelength shifted to smaller wavelengths at increased n values, which increased the Drude weight, as described in Eq. (2);[16,17] moreover, the SPRs of the armchair edge in the X-direction were stronger than those of the zigzag edge in the Y-direction.[19]

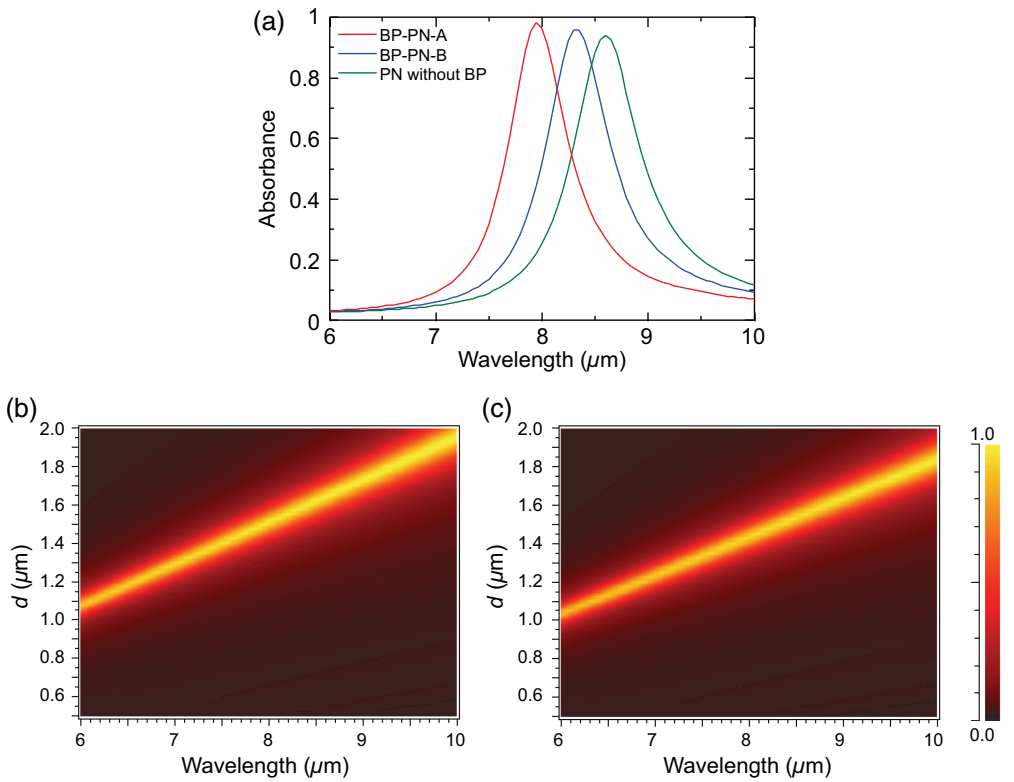

Fig. 5 (a) Calculated absorbance spectra with $d = 1.5$ μm for PN without BP, BP-PN-A, and BP-PN-B. Calculated absorbances as a function of wavelength and d for (b) BP-PN-A and (c) BP-PN-B. The color scale represents the absorbance.

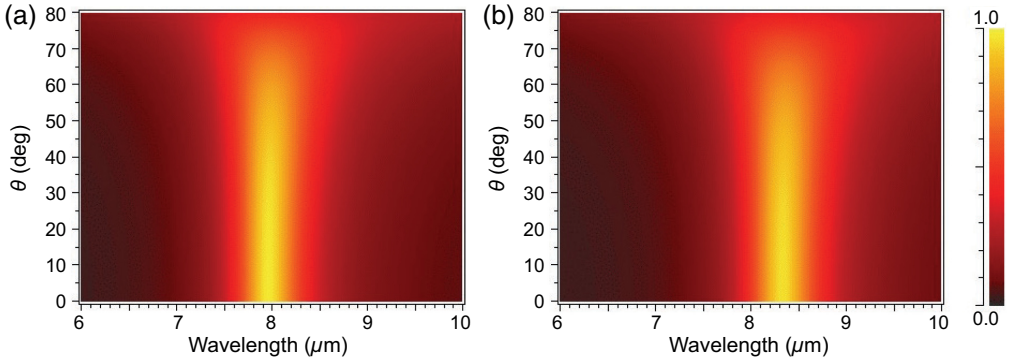

Fig. 6 (a) Calculated absorbances as a function of wavelength and θ for (a) BP-PN-A and (b) BP-PN-B. The color scale represents the absorbance.

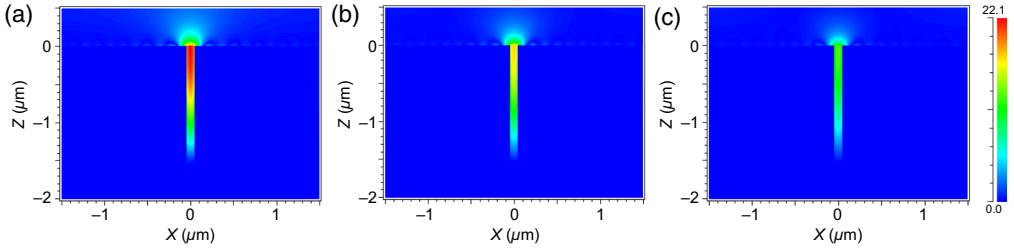

Fig. 7 Calculated electric field distributions at the wavelength of 8.00 μm with $d = 1.5$ μm for (a) BP-PN-A, (b) BP-PN-B, and (c) PN without BP. The color scale represents the amplitude of the electric field.

Figures 7(a)–7(c) present the electric field distributions at a wavelength of 8.00 μm with $d =$ 1.5 μm for BP-PN-A [Fig. 7(a)], BP-PN-B [Fig. 7(b)], and PN [Fig. 7(c)] without BP, respectively. As shown in Fig. 5(a), the maximum absorption was observed for BP-PN-A at a wavelength of 8.00 μm. It should be noted that the grating regions were masked to ensure visibility.

As shown in Figs. 7(a)–7(c), strong LSPR occurs in the groove of BP-PN-A, which is a unique characteristic of plasmonic nanogratings. However, the electric field enhancements in BP-PN-B and PN without BP were weaker than those in BP-PN-A. The order of enhancement corresponded to the absorbances shown in Fig. 5(a). It is difficult to determine the absorption percentages of BP and plasmonic nanograting. However, these results show that BP contributes to absorption and that the absorption of BP can be enhanced compared with that of BP without plasmonic nanogratings. Moreover, the electrical field was strongly localized on the BP within the small groove width of 100 nm. The localization area is smaller than the incident wavelength by a factor of >80. This localization profile can realize higher performance BP-based IR photodetectors with extremely small detector sizes because the dark current can be reduced considerably as the detector size decreases. Although the unique absorption characteristics of plasmonic nanogratings, such as absorption wavelength control by d and incident-angle insensitivity, can be maintained in hybrid BP plasmonic nanograting systems, the coupling of SPR between the plasmonic nanograting and BP can be tuned by the edge of the BP configuration and n.

4 Conclusions

In this study, hybrid BP and plasmonic nanograting systems were numerically investigated. Polarization-selective near-unity absorption with an absorbance of $>90\%$, incident-angle insensitivity, and wavelength control of d was demonstrated. The absorption of BP can be enhanced compared with that of BP without plasmonic nanogratings by strong LSPRs induced within a small groove area. Moreover, the configuration of the edges of BP, e.g., the armchair and zigzag, in the groove direction can modify the absorption wavelength because BP produces anisotropic SPRs according to its anisotropic edge structure. The asymmetric edge structure of the BP and asymmetric plasmonic nanogratings produce the asymmetric SPR coupling. This shows the unique aspect of the light–matter interaction based on the asymmetric atomic bonds and bulk structure. The absorption wavelength decreased owing to the effect of BP, and the wavelength shift was larger for the armchair edge normal to the groove direction than that for the zigzag edge normal to the groove direction. The wavelength shift could be controlled by n. The absorption wavelength shortened following an increase in n. Moreover, n could be controlled by the electrical gating of the BP, which implied the tunability of the detection wavelength by the electrical gating of the BP. These results can be attributed to the anisotropic SPR coupling between BP and the plasmonic nanogratings. The proposed methodology can therefore contribute to the development of high-performance BP-based polarization- and wavelength-selective IR photodetectors and enhance the advanced function of electrical tunability of the detection wavelength.

Disclosures

The authors have no disclosures to declare.

Code and Data Availability

All the data supporting the findings of this study are available in this article.

Acknowledgments

Part of this work was presented at the SPIE Defense + Security conferences in 2024.[29]

References

1. K. S. Novoselov et al., "Electric field effect in atomically thin carbon films," *Science* **306**(5696), 666–669 (2004).
2. K. S. Novoselov et al., "Two-dimensional gas of massless Dirac fermions in graphene," *Nature* **438**(7065), 197–200 (2005).

3. S. Ogawa, S. Fukushima, and M. Shimatani, "Hexagonal boron nitride for photonic device applications: a review," *Materials* **16**(5), 2005 (2023).
4. S. Ogawa, S. Fukushima, and M. Shimatani, "Hexagonal-boron nitride/graphene van der Waals heterostructure-based wavelength-selective infrared absorbers using plasmonic metasurfaces for multi-spectral infrared photodetectors," *J. Opt. Soc. Am. B* **39**(12), 3149–3158 (2022).
5. B. Radisavljevic et al., "Single-layer MoS2 transistors," *Nat. Nanotechnol.* **6**(3), 147–150 (2011).
6. X. Ling et al., "The renaissance of black phosphorus," *Proc. Natl. Acad. Sci. U. S. A.* **112**(15), 4523–4530 (2015).
7. X. Wang and S. Lan, "Optical properties of black phosphorus," *Adv. Opt. Photonics* **8**(4), 618–655 (2016).
8. F. H. L. Koppens et al., "Photodetectors based on graphene, other two-dimensional materials and hybrid systems," *Nat. Nanotechnol.* **9**(10), 780–793 (2014).
9. S. Fukushima et al., "Photogating for small high-responsivity graphene middle-wavelength infrared photodetectors," *Opt. Eng.* **59**(3), 037101 (2020).
10. S. Fukushima et al., "Carrier density modulation and photocarrier transportation of graphene/InSb heterojunction middle-wavelength infrared photodetectors," *Opt. Eng.* **59**(9), 097101 (2020).
11. M. Shimatani et al., "Photoswitching effect of graphene photogated diodes with interfacial layers," *J. Opt. Soc. Am. B* **40**(9), 2349–2355 (2023).
12. Q. Guo et al., "Black phosphorus mid-infrared photodetectors with high gain," *Nano Lett.* **16**(7), 4648–4655 (2016).
13. P. K. Venuthurumilli, P. D. Ye, and X. Xu, "Plasmonic resonance enhanced polarization-sensitive photodetection by black phosphorus in near infrared," *ACS Nano* **12**(5), 4861–4867 (2018).
14. H. Jiao et al., "HgCdTe/black phosphorus van der Waals heterojunction for high-performance polarization-sensitive midwave infrared photodetector," *Sci. Adv.* **8**(19), eabn1811 (2022).
15. X. Ye et al., "High-performance diodes based on black phosphorus/carbon nanomaterial heterostructures," *Nanoscale Adv.* **5**(9), 2427–2436 (2023).
16. L. Han et al., "Active tuning of midinfrared surface plasmon resonance and its hybridization in black phosphorus sheet array," *ACS Photonics* **5**(9), 3828–3837 (2018).
17. T. Liu et al., "Black phosphorus-based anisotropic absorption structure in the mid-infrared," *Opt. Express* **27**(20), 27618–27627 (2019).
18. T. Liu et al., "Tunable anisotropic absorption in monolayer black phosphorus using critical coupling," *Appl. Phys. Express* **13**(1), 012010 (2020).
19. H. Khalilzadeh, A. Habibzadeh-Sharif, and N. Anvarhaghighi, "Design of a broadband infrared absorber based on multiple layers of black phosphorus nanoribbons," *J. Opt. Soc. Am. B* **38**(12), 3920–3928 (2021).
20. G. Xiao et al., "Tunable and anisotropic perfect absorber using graphene-black phosphorus nanoblock," *Opt. Express* **30**(13), 23198–23207 (2022).
21. N. Feng et al., "Near-unity broadband infrared absorption in a graphene-black phosphorus bimodal triple-layer structure," *Opt. Mater. Express* **13**(6), 1535–1546 (2023).
22. T. Guo and C. Argyropoulos, "Hybrid graphene-plasmon gratings," *J. Appl. Phys.* **134**(5), 050901 (2023).
23. S. Ogawa et al., "Hybrid graphene-high-aspect ratio plasmonic nanograting systems," *J. Appl. Phys.* **135**(15), 153107 (2024).
24. S. Ogawa et al., "Wavelength selective uncooled infrared sensor by plasmonics," *Appl. Phys. Lett.* **100**(2), 021111 (2012).
25. J. Hao et al., "High performance optical absorber based on a plasmonic metamaterial," *Appl. Phys. Lett.* **96**(25), 251104 (2010).
26. N. S. Azar et al., "Light–matter interaction enhancement in anisotropic 2D black phosphorus via polarization-tailoring nano-optics," *ACS Photonics* **8**(4), 1120–1128 (2021).
27. S. Ogawa et al., "Absorption properties of simply fabricated all-metal mushroom plasmonic metamaterials incorporating tube-shaped posts for multi-color uncooled infrared image sensor applications," *Photonics* **3**(1), 9 (2016).
28. S. Ogawa, Y. Takagawa, and M. Kimata, "Broadband polarization-selective uncooled infrared sensors using tapered plasmonic micrograting absorbers," *Sens. Actuat. A* **269**, 563–568 (2018).
29. S. Ogawa et al., "Hybrid black phosphorus-plasmonic nanograting for high-performance infrared sensing," *Proc. SPIE* **13046**, 130461T (2024).
30. K. Ikeda et al., "Controlled thermal emission of polarized infrared waves from arrayed plasmon nanocavities," *Appl. Phys. Lett.* **92**(2), 021117 (2008).
31. F. Pardo et al., "Light funneling mechanism explained by magnetoelectric interference," *Phys. Rev. Lett.* **107**(9), 093902 (2011).
32. P. Bouchon et al., "Total funneling of light in high aspect ratio plasmonic nanoresonators," *Appl. Phys. Lett.* **98**(19), 191109 (2011).
33. S. Ogawa and M. Kimata, "Direct fabrication and characterization of high-aspect-ratio plasmonic nanogratings using tapered-sidewall molds," *Opt. Mater. Express* **7**(2), 633–640 (2017).

34. N. Mattiucci et al., "Taming the thermal emissivity of metals: a metamaterial approach," *Appl. Phys. Lett.* **100**(20), 201109 (2012).
35. M. G. Moharam et al., "Formulation for stable and efficient implementation of the rigorous coupled-wave analysis of binary gratings," *J. Opt. Soc. Am. A* **12**(5), 1068–1076 (1995).
36. Z. Liu and K. Aydin, "Localized surface plasmons in nanostructured monolayer black phosphorus," *Nano Lett.* **16**(6), 3457–3462 (2016).
37. T. Low et al., "Tunable optical properties of multilayer black phosphorus thin films," *Phys. Rev. B* **90**(7), 075434 (2014).
38. J. Wang and Y. Jiang, "Infrared absorber based on sandwiched two-dimensional black phosphorus metamaterials," *Opt. Express* **25**(5), 5206–5216 (2017).
39. Y. Xu et al., "Triple-band black-phosphorus-based absorption using critical coupling," *Appl. Opt.* **59**(28), 9003–9009 (2020).
40. C. K. Lee et al., "Monatomic chemical-vapor-deposited graphene membranes bridge a half-millimeter-scale gap," *ACS Nano* **8**(3), 2336–2344 (2014).
41. A. D. Rakic et al., "Optical properties of metallic films for vertical-cavity optoelectronic devices," *Appl. Opt.* **37**(22), 5271–5283 (1998).

Biographies of the authors are not available.